crystals

MDPI

Article

Real Space Quantum Cluster Formulation for the Typical Medium Theory of Anderson Localization

Ka-Ming Tam [1,2,*], Hanna Terletska [3,*], Tom Berlijn [4], Liviu Chioncel [5,6] and Juana Moreno [1,2]

1 Department of Physics and Astronomy, Louisiana State University, Baton Rouge, LA 70803, USA; moreno@phys.lsu.edu
2 Center for Computation & Technology, Louisiana State University, Baton Rouge, LA 70803, USA
3 Department of Physics and Astronomy, Middle Tennessee State University, Murfreesboro, TN 37132, USA
4 Center for Nanophase Materials Sciences, Oak Ridge National Laboratory, Oak Ridge, TN 37831, USA; tberlijn@gmail.com
5 Theoretical Physics III, Center for Electronic Correlations and Magnetism, Institute of Physics, University of Augsburg, D-86135 Augsburg, Germany; liviu.chioncel@physik.uni-augsburg.de
6 Augsburg Center for Innovative Technologies, University of Augsburg, D-86135 Augsburg, Germany
* Correspondence: phy.kaming@gmail.com (K.-M.T.); Hanna.Terletska@mtsu.edu (H.T.)

Abstract: We develop a real space cluster extension of the typical medium theory (cluster-TMT) to study Anderson localization. By construction, the cluster-TMT approach is formally equivalent to the real space cluster extension of the dynamical mean field theory. Applying the developed method to the 3D Anderson model with a box disorder distribution, we demonstrate that cluster-TMT successfully captures the localization phenomena in all disorder regimes. As a function of the cluster size, our method obtains the correct critical disorder strength for the Anderson localization in 3D, and systematically recovers the re-entrance behavior of the mobility edge. From a general perspective, our developed methodology offers the potential to study Anderson localization at surfaces within quantum embedding theory. This opens the door to studying the interplay between topology and Anderson localization from first principles.

Keywords: metal insulator transition; Anderson localization; random disorder; typical medium theory; dynamical mean field theory; coherent potential approximation; dynamical cluster approximation; cellular dynamical mean field theory; cluster mean field theory

Citation: Tam, K.-M.; Terletska, H.; Berlijn, T.; Chioncel, L.; Moreno, J. Real Space Quantum Cluster Formulation for the Typical Medium Theory of Anderson Localization. *Crystals* **2021**, *11*, 1282. https://doi.org/10.3390/cryst11111282

Academic Editor: Andrej Pustogow

Received: 17 September 2021
Accepted: 15 October 2021
Published: 22 October 2021

1. Introduction

The localization problem in disordered electronic systems was introduced in Anderson's seminal paper [1] in the late fifties, and it still remains in the forefront of research in materials science and condensed matter physics [2–5].

In disordered media, the scattering of charge carriers off random impurities may inhibit their propagation across the sample leading to a spatial confinement of carriers, a phenomenon known as Anderson localization [1]. Weak localization and strong Anderson localization have been conjectured and subsequently observed in experiments [6–10]. As a wave phenomenon, Anderson localization has been demonstrated for electrons [11–16], sound [17], photons [18–25], and ultra cold atoms [26].

To model disorder, Anderson proposed a simplified model of electrons hopping between lattice sites being subject to static scattering processes on locally disordered centers. The stochastic character of the problem is encoded into the on-site energies (disordered scattering centers) considered as random variables distributed according to a chosen probability distribution. The Green's function imaginary part, the local density of states (LDOS), turns out to be an important quantity which characterizes the disordered system. For example, the LDOS is finite for extended states, while the spectrum of localized states is discrete. A decade later, an approach based on the distribution of the site and energy dependent self-energies was formulated [27]. This approach leads to a self-consistent

equation for the self-energy, which can be solved on a Cayley tree (Bethe lattice). However, for general lattices, only an approximate solution can be provided.

Computations for substitutionally disordered three-dimensional materials with ordinary lattice structures are therefore difficult to perform within the framework of tight-binding models [1,27]. Suitable modeling in such cases can be constructed based on effective medium theories. Among them, single site effective medium methods, such as the coherent potential approximation (CPA) [28–35] and the typical medium theory (TMT) [36], proved to be simple and transparent theories that are able to capture important features of the disorder effects in electron systems. Common to these two methods is the mapping of the lattice problem into the impurity placed in a self-consistently determined effective medium. In both methods, the measured quantity is the disorder averaged Green's function; however, in CPA, the Green's function is linearly (algebraically) averaged, while, in the TMT, the geometric average of the LDOS is used. This difference in disorder averaging defines the average and the typical effective media, respectively.

Unlike the algebraically averaged Green's function of the CPA effective medium, the geometric averaged LDOS, called the typical density of states (TDOS), drops to zero [36–47], at the Anderson transition. The geometrically averaged TDOS is an approximation to the most probable value in the distribution of the LDOS. At the Anderson transition, the system is not self-averaged, hence the distribution of the LDOS is highly skewed with long tails [37,48]. Therefore, the average and most probable values of the LDOS will be very different close to the transition [37,49–51]. Dobrosavljevic et al. [36] incorporated such statistical properties of the LDOS within an effective medium approach, called the TMT. They showed that the TDOS successfully captures the main signatures of the Anderson localization transition, with the TDOS being an order parameter to detect the localized states. In Refs. [52–54], the momentum-space cluster extension of the TMT [54], the typical medium dynamical cluster approximation (TMDCA) has been developed. The TMDCA is the typical medium extension of the Dynamical Cluster Approximation (DCA) [55,56], a momentum-space cluster extension of the CPA. The TMDCA overcomes the shortcomings of the local single site TMT and accurately predicts the critical disorder strength of the Anderson localization transition in a single-band Anderson model. For model Hamiltonian systems, the TMDCA has been applied to non-interacting and weakly interacting disordered three-dimensional systems [52,53,57,58], systems with off-diagonal disorder [59], phonon localization [60,61], and multi-orbital models [62]. Some of the methods inspired by the typical medium theories have been combined with first-principles calculations [63–65].

Complementary to the momentum space cluster methods, described above, techniques using embedding in real space provide an interesting alternative. This constitutes the aim of the present work. We have previously formulated the embedding into the effective typical medium which allows for addressing the Anderson localization transition in the framework of a locally self-consistent approach [66]. In addition, the locally self-consistent formulation opens up the possibility to formulate linear scaling methods. Unlike the previous typical medium cluster extensions of TMT, formulated in the momentum space (TMDCA) [54,67], or in a mixed representation (locally self-consistent approach) [66,68], here we propose an exclusively real space cluster extension of TMT (cluster-TMT). This construction is formally equivalent to the real space cluster extension of the dynamical mean field theory (DMFT) [69–73].

The key accomplishment of the present study is the development of a cluster mean field theory for the description of Anderson localization. The developed cluster version is based on a real-space approach, and presents an alternative to the existing momentum space version of TMDCA. To demonstrate the validity of the method, we apply it to the three-dimensional Anderson model with box disorder distribution, and reproduce the full phase diagram and the critical disorder strength, W_c, for the metal-insulator transition. The cluster mean field theory we designed is an extension of the local single site typical medium theory. The developed real space cluster extension method incorporates the spatial non-local effects systemically; therefore, the re-entrance behavior of the 3D Anderson model is recovered.

We find that cluster extensions of TMT are necessary to properly capture the non-local effects in the Anderson transition. Quantitatively, our results are in good agreement with the existing data in the literature. In particular, we find that the converged cluster value of $W_c \approx 17.05$ is superior to the value of 13.4 provided by single site TMT calculations. We demonstrate that non-local spatial correlations are significant in the 3D Anderson model, and hence going beyond a single site approximation is necessary to properly describe the metal-insulator transition. Unlike the single site TMT, the present real-space cluster computation captures the re-entrance behavior driven by non-local multiple scattering effects which are missing in local approximations [5,36,48,74]. In addition, just like the TMDCA, the real space cluster-TMT allows for a computationally efficient treatment of the non-local effects in Anderson localization. In addition, however, the real-space cluster TMT opens the door to treating problems with open boundary conditions, which offers the possibility to study the localization of surface states. One potential application of this capability would be the search for a material realization of the topological Anderson insulator [75] via first principles calculations. In addition, the presented formalism being a real space cluster opens venues for an easier embedding with ab initio Green's function electronic structure methods, which offer a more natural approach (in contrast to the momentum space TMDCA) to disordered real materials, including high entropy alloys and disordered metals [63–65].

It is worth noting that there is a long history of applications of the CPA both as a tool for model calculations and in computational studies of real materials. We refer the interested readers to the review of Yonezawa and Morigaki [76]. An extensive review of the early development of the DMFT method can be found in Georges et al. [77], and a review of more recent cluster extensions can be found in Maier et al. [78]. A review of current research on the Anderson localization using cluster methods can be found in Terletska et al. [54].

This paper is organized as follows: in Section 2, we present the Anderson model. In Section 3, we first briefly review the algorithm of the single site TMT and discuss the algorithm for the real-space cluster extension of the TMT. In Section 4, we present the results obtained with our cluster-TMT for the 3D Anderson model with box disorder distribution. We conclude in Section 5 and discuss possible future developments.

2. Model

Anderson proposed [1] that non-interacting electrons on site-disordered lattices may localize because of the destructive interference of wave functions. Subsequent theoretical and numerical studies [79] support the picture that, in three dimensions and for large enough disorder strength, single particle wave functions are localized and decay exponentially on the scale of the localization length.

The Anderson model Hamiltonian has the form:

$$H = -t \sum_{<i,j>,\sigma} (c^{\dagger}_{i\sigma} c_{j\sigma} + H.c.) + \sum_{i,\sigma} V_i n_{i\sigma}, \tag{1}$$

where $c^{\dagger}_{i\sigma}$ and $c_{i\sigma}$ are the creation and annihilation operators for electrons at site i with spin σ. $n_{i\sigma}$ is the number operator for site i of spin σ; t is the hopping energy between nearest neighbors. We consider a 3D simple cubic lattice. We set $t = 1$ to serve as the energy scale. The local random disorder is given by V_i. Here, we consider a so-called box disorder with $P(V_i) = \frac{1}{W}\Theta(W - V_i)$. This allows the disorder strength to be characterized by W. Other distributions are also considered in the literature; some common ones included bi-modal, Gaussian, and Lorentzian distributions [53,80].

The Anderson model has been the focus of numerous studies of the disorder-induced electron localization. Highly accurate numerical calculations based on the transfer matrix method and multifractal analysis have been used to study the model extensively, especially for zero energy [5,74,81–90].

Relatively few studies have been devoted to energy away from zero. A prominent feature at higher energy is the re-entrance from a metal to an insulator to a metal, as the disorder strength increases [74,82,91,92]. A heuristic argument for the nature of the re-entrance behavior is based on the tunneling mechanism for energies beyond the bandwidth of the hopping model. The width of the density of states increases as the disorder increases, though the states are localized. At sufficiently large disorder, the localized density of states is large enough to allow tunneling. The tunneling could become sufficiently long range that the localized states become extended, thus the insulator becomes a metal. This explains the lower transition in the re-entrance. Further increasing the disorder strength, the localized state will be more sparse in energy and tunneling becomes less likely to happen and insulating state resumes.

The above argument depends on the distribution of disorder, and the tunneling effect is maximised when the localized states are close in energy. A bounded random distribution is favored as compared to other distributions which are more widely spread over a range of energies, such as the Lorentzian distribution. The tunneling argument can only be supported in a system with multiple sites. For example, the TMT, which is a single site approximation, does not capture the re-entrance behavior. Thus, the capability of describing the re-entrance can serve as a good test for our real space cluster-TMT.

3. The Real Space Quantum Cluster Extension of TMT

3.1. Typical Medium Theory: TMT

To set the stage for the discussion of the real-space cluster extension of the TMT, here we briefly review the main steps of the TMT analysis. The TMT can be considered as a typical medium generalization of the CPA [28–34]. In a similar way to the CPA, the TMT employs the mapping of the original lattice problem into the impurity placed in a self-consistently determined effective medium. However, in the TMT, the typical (geometrically averaged over disorder) local density of states is used to construct the mean field bath for the effective impurity problem.

The numerical algorithm for the TMT procedure is shown in Figure 1. First, the guess for the effective medium self-energy $\Sigma(\omega)$ is made, usually zero. Then, the local (coarse-grained) lattice Green's function is calculated as $\bar{G}(\omega) = \frac{1}{N}\sum_k \frac{1}{\omega - \epsilon_k - \Sigma(\omega)}$. Using the Dyson's equation, we then obtain the impurity-excluded Green's function (bath Green's function) $\mathcal{G}^{-1}(\omega) = \bar{G}^{-1}(\omega) + \Sigma(\omega)$.

The next step is to solve the impurity problem. For each randomly chosen disorder configuration V, we calculate the impurity Green's function $G_{imp}(\omega, V) = (\mathcal{G}^{-1}(\omega) - V)^{-1}$. From this quantity, we obtain the typical (geometrically averaged density of states) $\rho_{typ}(\omega)$, which is constructed as $\rho_{typ}(\omega) = e^{\langle ln(\rho(\omega,V))\rangle}$. Here, $\rho(\omega, V) = -\frac{1}{\pi}\Im G_{imp}(\omega, V)$, and $\langle \ldots \rangle$ stands for the disorder averaging. In general, the geometrical average is not equivalent to the typical value. However, for log-normal distributions, the geometrical average is the same as the typical value and, since numerical studies have shown that near the localization transition the local density of states is log-normal distributed [37], this assumption is appropriate.

The output of the TMT impurity solver is the typical Green's function which is obtained using the Hilbert transform: $G_{typ}(w) = \frac{1}{\pi}\int d\omega' \frac{\rho_{typ}(\omega')}{\omega - \omega'}$. This step is the only difference between the CPA and the TMT self-consistency loop. For example, in the CPA, instead of the typical, the algebraically average DOS is calculated $\rho_{ave} = \langle \rho(\omega, V) \rangle$, with the average Green's function $G_{ave}(w) = \frac{1}{\pi}\int d\omega' \frac{\rho_{ave}(\omega')}{\omega - \omega'}$ being the output of the CPA impurity solver. Note that, for the CPA case, one can just do the disorder averaging over Green's function without the Hilbert transform of the average density.

Finally, the TMT self-consistency loop is closed by getting a new estimate of the self-energy $\Sigma(\omega) = \mathcal{G}^{-1}(\omega) - G_{typ}^{-1}(\omega)$, which is then used to calculate the coarse-grained local lattice Green's function. The whole procedure then repeats, until convergence is

reached at which the impurity and the local lattice Green's function are equal within the desired accuracy.

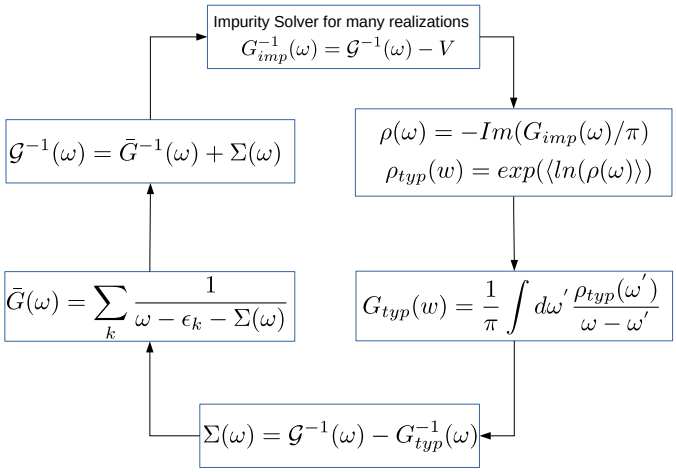

Figure 1. Numerical algorithm for the typical medium theory.

3.2. Real Space Cluster-TMT

To properly capture the effect of multiple impurities scattering in the disorder-driven Anderson localization, the cluster extension of the TMT is needed. Here, we present the real-space cluster extension of the TMT. Such real space variant of the cluster extension of the TMT is formally equivalent to the cluster DMFT solver, which has been extensively used in strongly-correlated electron systems to study non-local effects beyond DMFT. Here, we use the cluster DMFT approach as a tool to capture spacial non-local correlations beyond the TMT in disordered non interacting systems.

In the real space cluster-TMT, the infinite lattice in real space is tiled with identical clusters of size N_c [93]. In such construction, the scattering of electrons by impurities within a cluster is treated exactly, while the effects of impurities outside the cluster are replaced by the non-disordered effective medium (bath) that is determined self-consistently. There is no implicit assumption that the translational invariance is obeyed within the cluster. Therefore, the Green's function of the cluster is represented by an $N_c \times N_c$ matrix, which we denote as $\hat{G}_c(\omega)$. For the same reason, the self-energy and the bath Green's function are also represented in terms of matrices.

The self-consistency procedure for our real space cluster-TMT is shown in Figure 2. First, we start with the guess of the self-energy matrix $\hat{\Sigma}(\omega)$ (usually zero). Then, we calculate the lattice Green's function projected onto the cluster space $\hat{\bar{G}}(\omega) = \frac{N_c}{N}\sum_{\mathbf{k}\in R.B.Z.}[\omega - \hat{t}(\mathbf{k}) - \hat{\Sigma}(\omega)]^{-1}$, where R.B.Z. stands for the reduced Brillouin Zone of the cluster with $-\frac{2\pi}{L_c} < k_x, k_y, k_z < \frac{2\pi}{L_c}$. In addition, $\hat{t}(\mathbf{k})$ is the dispersion of the lattice model expressed as a partial Fourier transform over the reduced Brillouin zone. Any element of this dispersion matrix is given as $t_{\mathbf{r},\mathbf{r}'}(\mathbf{k}) \equiv \sum_{\mathbf{R}} exp(i\mathbf{k}\cdot(\mathbf{R} + \mathbf{r} - \mathbf{r}'))t_{\mathbf{r},\mathbf{r}'+\mathbf{R}}$, where $\mathbf{R}$ is the location vector of the super-cell, and $\mathbf{r}$ and $\mathbf{r}'$ are the vectors for the location of each site within a super-cell [93].

Next, using the Dyson's equation, we calculate the bath Green's function matrix, $\hat{\mathcal{G}}^{-1}(\omega) = \hat{\bar{G}}^{-1}(\omega) + \hat{\Sigma}(\omega)$, which is used to construct the cluster problem. Then, for each disorder configuration V, we calculate the cluster Green's function by solving the matrix equation $G_c^{-1}(\omega, i, j) = \mathcal{G}^{-1}(\omega, i, j) - V(i, j)\delta_{ij}$.

The key to incorporate the typical medium into the analysis is to connect the Green's function matrix to the typical density of states. For this, we generalize the procedure we

used for the multi-orbital problem of the TMDCA [62], and define the typical density of states matrix in a similar way:

$$\hat{\rho}_{typ}(\omega) \equiv \begin{pmatrix} e^{\langle |\ln \rho_{11}(\omega)| \rangle} \frac{\langle \rho_{11} \rangle}{\langle |\rho_{11}| \rangle} & \cdots & e^{\langle \ln |\rho_{1N_c}(\omega)| \rangle} \frac{\langle \rho_{1N_c} \rangle}{\langle |\rho_{1N_c}| \rangle} \\ . & . & . \\ . & . & . \\ . & . & . \\ e^{\langle \ln |\rho_{N_c1}(\omega)| \rangle} \frac{\langle \rho_{N_c1} \rangle}{\langle |\rho_{N_c1}| \rangle} & \cdots & e^{\langle \ln |\rho_{N_cN_c}(\omega)| \rangle} \frac{\langle \rho_{N_cN_c} \rangle}{\langle |\rho_{N_cN_c}| \rangle} \end{pmatrix}, \quad (2)$$

Here, the diagonal entries will be just equal to $e^{\langle \rho_{ii}(\omega) \rangle}$ because $\rho_{ii} > 0$ is always positive definite; $\rho_{ii} = -\frac{1}{\pi}\Im[G_{ii}(\omega)]$; and for the off-diagonal terms $\rho_{ij} = \frac{i}{2\pi}[G_{ij}(\omega) - G_{ji}(\omega)]$ [94]. The role of the non-local off-diagonal components in the geometrically averaged cluster Green's function is explained in the Appendix A.

Notice that the real space cluster extension of the CPA, with the average effective medium, can be obtained by replacing the typical DOS with the linearly average DOS in the above Equation (2), i.e.,

$$\hat{\rho}_{ave}(\omega) \equiv \begin{pmatrix} \langle \rho_{11}(\omega) \rangle & \cdots & \langle \rho_{1N_c}(\omega) \rangle \\ . & . & . \\ . & . & . \\ . & . & . \\ \langle \rho_{N_c1}(\omega) \rangle & \cdots & \langle \rho_{N_cN_c}(\omega) \rangle \end{pmatrix}. \quad (3)$$

The $\hat{\rho}_{typ}(\omega)$ of Equation (2) possesses the following properties: (1) for $N_c = 1$, it reduces to the local TMT with $\rho_{typ}(\omega) = e^{\langle |ln\rho(\omega)| \rangle}$; (2) At small disorder strength $W \ll W_c$, we observe numerically that $< \ln \rho(\omega) > \approx \ln < \rho(\omega) >$, i.e., the typical density of states (DOS) reduces to the average DOS calculated using algebraic averaging over disorder: $\rho_{typ} \to \rho_{ave}(\omega)$. Hence, in this regime, the typical DOS obtained with the cluster-TMT is expected to be close in magnitude to the one obtained with the real-space cluster-CPA with averaged effective medium. Such real space cluster extension of CPA is different from other existing cluster extensions, including the DCA [55,56] and non-local CPA [95]. The difference is that, in the real space cluster-CPA, all the quantities are matrices in the real space, and the coarse-graining step for $\hat{\bar{G}}$ uses a projected lattice dispersion which is constrained to the real space cluster space.

In the next step of the cluster-TMT self-consistency loop, we must calculate the cluster typical Green's function $\hat{G}_{typ}$ ($\hat{G}_{ave}$ for the cluster-CPA) using the Hilbert transform. The Hilbert transform is performed for each matrix element individually, $G_{typ,ij}(w) = \frac{1}{\pi}\int d\omega' \frac{\rho_{typ,ij}(\omega')}{\omega - \omega'}$.

Next, using the Dyson's equation, we get the updated self-energy $\hat{\Sigma}(\omega) = \hat{\mathcal{G}}^{-1}(\omega) - \hat{G}^{-1}_{typ}(\omega)$, which is then used to calculate the coarse-grained lattice Green's functions matrix $\hat{\bar{G}}$. The whole procedure then repeats, until convergence is reached with the desired accuracy.

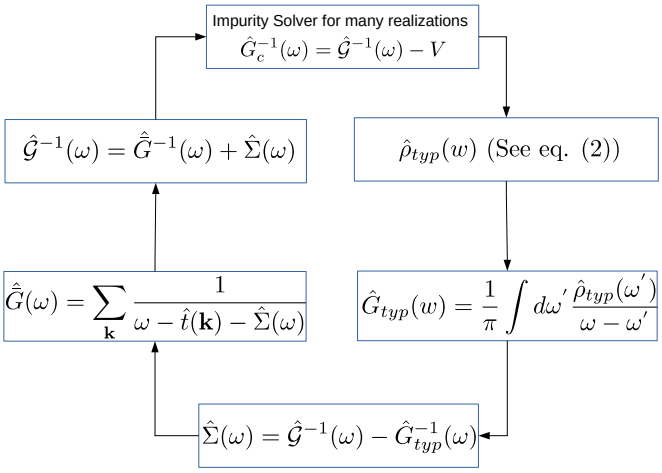

Figure 2. The self-consistency algorithm for the real space cluster-TMT formalism.

4. Results

We start the discussion of our results for the 3D Anderson model (for a box disorder distribution) by first focusing in panel a of Figure 3. This panel displays the $N_c = 3^3$ cluster average DOS (ADOS=$\frac{1}{N_c}\Sigma_i(\frac{-1}{\pi})\Im\hat{G}_{c,ii}(\omega)$) obtained using the average effective medium (constructed from Equation (3)) in the cluster self-consistent loop. These results correspond to the real-space cluster extension of the CPA. The data show that, as disorder strength W increases, the ADOS broadens and gets smaller, but does not go through significant qualitative changes when the metal-insulator transition is approached.

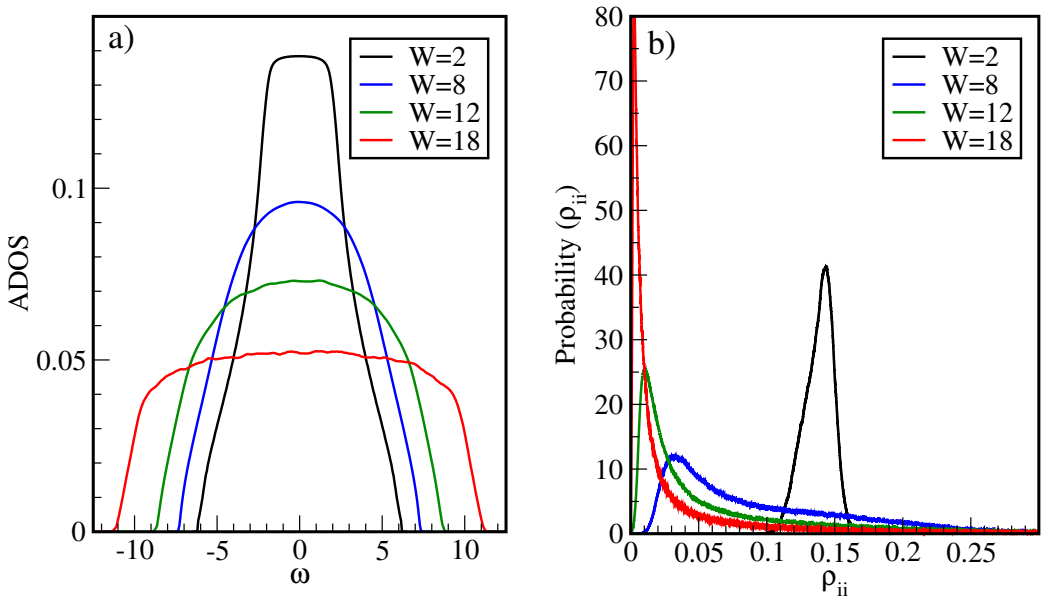

Figure 3. (**a**) The ADOS calculated for $N_c = 3^3$ at several disorder strengths $W = 2, 8, 12, 18$; (**b**) the probability distribution function of the local density of states ρ_{ii} for several values of disorder strengths, $W = 2, 8, 12, 18$.

To demonstrate why the ADOS fails to describe the Anderson transition, we display the probability distribution of the local density of states in panel b of Figure 3. At small disorder $W = 2$, the distribution of the LDOS is Gaussian-like. However, as disorder strength increases, the probability distribution becomes skewed with long tails (indicating that the system is not self-averaging). At even larger disorder strength ($W = 18$), the probability distribution peaks at values very close to zero. Such skewness of the distribution

functions for large disorder strengths implies that the average and the most probable (typical) values of the DOS will differ significantly, and hence the numerical algorithms that employ the globally averaged Green's function in the self-consistency loop (e.g., the CPA, the DCA) will fail to describe the Anderson transition.

These results clearly demonstrate that the typical medium treatment is required to capture the non self-averaging behavior through the Anderson transition. To show this, in Figure 4, we compare the data for the energy resolved ADOS and the TDOS calculated for a cluster of $N_c = 3^3$ sites. The $\mathrm{TDOS}(\omega) = exp(\frac{1}{N_c}\Sigma_i ln((\frac{-1}{\pi})\Im \tilde{G}_{c,ii}(\omega)))$ is obtained from the present real-space cluster-TMT procedure which employs the geometric averaging in the self-consistency loop. At weak disorder strength $(W = 2.5)$, as expected from our analytical arguments, both ADOS and TDOS are practically the same, indicating that, when $W \ll W_c$, the real space cluster-TMT reduces to the cluster-CPA scheme. As disorder strength increases, the ADOS and TDOS behave very differently. While the $\mathrm{ADOS}(\omega)$ broadens and remains finite, the $\mathrm{TDOS}(\omega)$ gets continuously suppressed $(W = 10)$ and vanishes at even larger disorder strength $(W = 16)$. Such vanishing of the TDOS at strong disorder values indicates that geometrically average DOS can be used as an order parameter for the Anderson localized states.

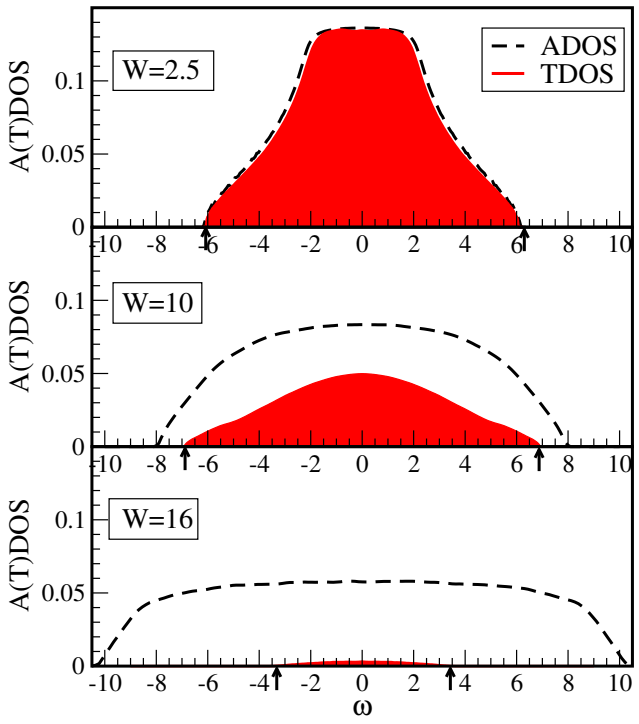

Figure 4. Evolution of the ADOS (dash lines) and the TDOS (shaded areas) as function of frequency ω at different disorder strengths $W = 2.5, 10, 16$, calculated using a cluster of $N_c = 3^3$. The approximate positions of the mobility edge boundaries are marked by vertical arrows.

Notice that, below the Anderson transition, for $W \ll W_c$, localization of states starts at the band tails. This is indicated by the vanishing $\mathrm{TDOS}(\omega)$ and the finite $\mathrm{ADOS}(\omega)$ at higher frequencies ω. The mobility edge (shown by arrows), i.e., the energy which separates the extended (with a finite TDOS) from the localized states (with zero TDOS) follows the expected re-entrance trajectory [52]: the mobility edge first expands beyond the zero disorder edge boundary, and then retracts at larger disorder strengths.

Next, we consider the evolution of the critical disorder strength W_c for the Anderson transition as a function of the cluster size N_c. The critical disorder W_c is extracted from the vanishing TDOS at the band center $(\mathrm{TDOS}(\omega = 0))$. In Figure 5, we plot $\mathrm{TDOS}(\omega = 0)$ as a function of disorder strength W for several cluster sizes $N_c = 1, 2, 3, 2^3, 3^3, 4^3$. For $N_c = 1$ (the local TMT case), the critical disorder is $W_c \approx 13.4$. Since TMT is a mean field theory, it

is expected that the critical disorder strength is underestimated and thus it is lower than the exact value. As the cluster size N_c increases, more spatial fluctuations are taken into account, which improves the value of W_c. With increasing N_c, the W_c converges quickly to $W_c \approx 17.05$ (see the inset of Figure 5), which is in good agreement with the values of W_c reported in the literature [90]. In addition, notice that, unlike the TDOS, the ADOS$(w = 0)$ (shown by the dashed line in Figure 5) remains finite as the disorder strength W increases, indicating that it can not be used as an order parameter for the Anderson transition, and hence the typical medium treatment is needed.

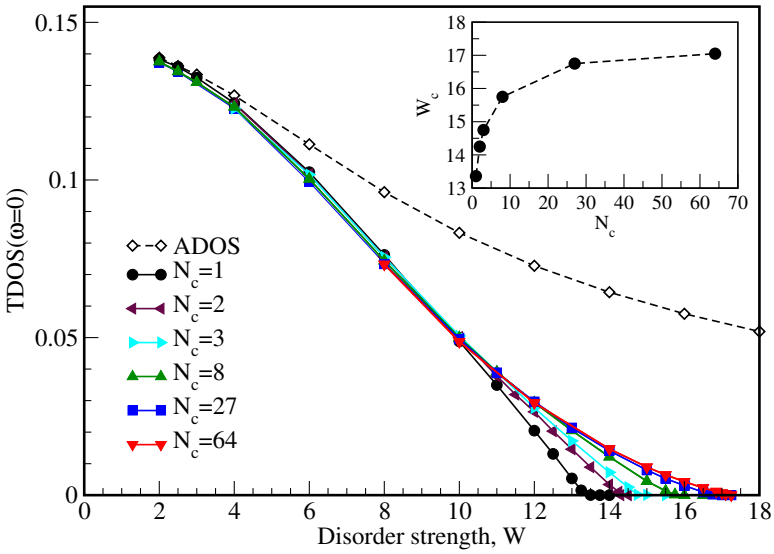

Figure 5. The typical density of states (solid lines) at the band center, $TDOS(\omega = 0)$, as a function of disorder strength W calculated for different cluster sizes $N_c = 1, 2, 3, 8, 27, 64$. The ADOS$(\omega = 0)$ as a function of disorder strength W is obtained for $N_c = 4^3$ (dashed line). Inset: the cluster size N_c dependence of the critical disorder strength W_c determined from the vanishing TDOS$(\omega = 0)$.

Finally, in Figure 6, we present the disorder strength W vs. frequency ω phase diagram. Here, we plot the cluster size N_c dependence of the mobility edge boundaries at different disorder strengths W obtained by our real space cluster-TMT formalism. In addition, we also show the band edges, which are defined by the frequencies at which ADOS$(w) = 0$. As we discussed above, a signature of the cluster mean field theory is the re-entrance at high energy. At $N_c > 1$, the mobility edge boundaries first expand and then retract back with increasing W. As Figure 6 displays, such re-entrance behavior is missing in the single site ($N_c = 1$) TMT case, and is recovered for $N_c > 1$ clusters. This indicates that non-local spacial correlations and multiple-scattering effects in the Anderson transition are important, and capturing such effects requires the usage of finite cluster methods. To benchmark our results even further, we also present the mobility edge trajectories obtained from the highly accurate transfer matrix method (TMM) [54]. For $N_c = 4^3$, the cluster-TMT results are already rather close to those of the TMM. These results demonstrate that our cluster-TMT method can be used to successfully describe the electron localization in the 3D Anderson model.

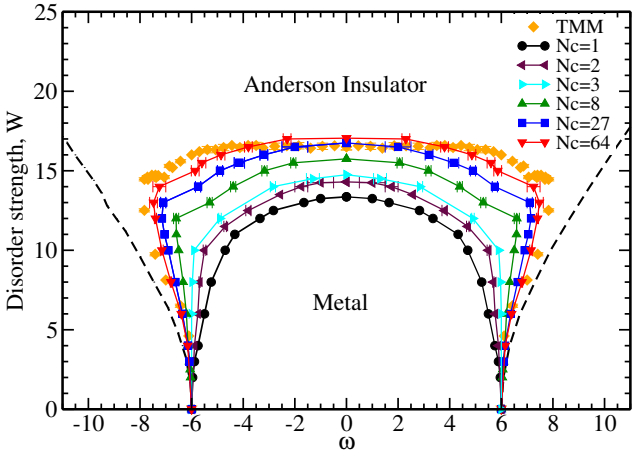

Figure 6. Disorder strength W vs. frequency ω phase diagram of 3D Anderson model obtained from cluster-TMT calculations. The mobility edge boundaries (solid lines) are obtained for $N_c = 1, 2, 3, 8, 27, 64$ cluster sizes. The dashed lines mark the band edges obtained from the ADOS(ω). The transfer matrix method (TMM) mobility edge boundaries are taken from Ref. [52].

5. Conclusions

We develop a real space quantum cluster theory based on the typical medium theory for random disorder systems. Unlike the coherent potential approximation with the algebraically average effective medium, the TMT captures the localization transition by considering the geometrically averaged local density of states to construct an effective medium. However, being a single site theory, the TMT underestimates the critical disorder strength of the transition, and misses the re-entrance behavior, which is due to the combined effects from multiple scattering sites. Recent studies based on the dynamical cluster approximation already confirmed that such non-local effects can be captured by considering momentum-space clusters extension of TMT [54].

In this paper, we construct the real space variant of the cluster-TMT. This method by construction is similar to the cellular dynamical mean field theory [72], which is a popular cluster method effectively used for strongly interacting electron systems. Here, we adopt such a real space cluster approach to disordered systems. Applying our real-space cluster-TMT approach to the 3D Anderson model with a box distribution, we demonstrate that the cluster-TMT is a successful self-consistent numerical approach to capture the Anderson localization transition. Performing N_c cluster-size analysis, we demonstrate the importance of including non-local spacial effects to properly describe the Anderson localization physics. Quantitatively, our results are in good agreement with existing data; in particular, we find that the converged cluster value of $Wc^{cluster-TMT} \approx 17.05$ is superior to the value predicted by single-site TMT, $W^{TMT} \approx 13.4$. Unlike the single site approach, the present real-space cluster-TMT captures the re-entrance behavior and correctly reproduces the phase diagram of the 3D Anderson model. The method, in principle, can also be used to calculate two particle quantities [96]. Furthermore, while the cluster TMT in this study has been restricted to periodic boundary conditions, the same methodology can be used to simulate Anderson localization in surfaces. This will be relevant, for example, to unraveling the role of disorder in topological materials [75,97]. Another interesting topic is to combine this approach with the multiple scattering theory [58], and the locally self-consistent multiple scattering method [66] for the study of materials with random disorder.

Author Contributions: Investigation, K.-M.T., H.T., T.B., L.C. and J.M.; Writing—original draft, K.-M.T. and H.T.; Writing—review & editing, K.-M.T., H.T., T.B., L.C. and J.M. All authors have read and agreed to the published version of the manuscript.

Funding: This manuscript is based upon work supported by the U.S. Department of Energy, Office of Science, Office of Basic Energy Sciences under Award Number DE-SC0017861. This work used the high performance computational resources provided by the Louisiana Optical Network Initiative http://www.loni.org, accessed on 16 September 2021, and HPC@LSU computing. This work also used the Extreme Science and Engineering Discovery Environment (XSEDE) through allocation DMR130036. K.-M.T. is partially supported by NSF DMR-1728457 and NSF OAC-1931445. H.T. has been supported by NSF OAC-1931367 and NSF DMR-1944974 grants. L.C. acknowledges the financial support by the Deutsche Forschungsgemeinschaft through TRR80 (project F6) project No. 107745057. A portion of this research was conducted at the Center for Nanophase Materials Sciences, which is a DOE Office of Science User Facility (TB). The manuscript has been authored by UT-Battelle, LLC under Contract No. DE-AC05-00OR22725 with the U.S. Department of Energy. The United States Government retains and the publisher, by accepting the article for publication, acknowledges that the United States Government retains a non-exclusive, paid-up, irrevocable, worldwide license to publish or reproduce the published form of this manuscript, or allow others to do so, for United States Government purposes. The Department of Energy will provide public access to these results of federally sponsored research in accordance with the DOE Public Access Plan (http://energy.gov/downloads/doe-public-access-plan, accessed on 16 September 2021).

Institutional Review Board Statement: Not applicable.

Informed Consent Statement: Not applicable.

Data Availability Statement: Correspondence and requests for data should be addressed to K.-M.T. or H.T.

Acknowledgments: The authors would like to thank V. Dobrosavljevic and S. Iskakov for useful comments and discussions.

Conflicts of Interest: The authors declare no conflict of interest.

Appendix A

In this section, we discuss the role of the non-local off-diagonal components in the ansatz for the geometrically averaged cluster Green's function of Equation (2). For this, we consider the "local" ansatz given by Equation (A1), where we set all off-diagonal terms in the typical DOS equal to zero:

$$\hat{\rho}_{typ}^{local}(\omega) \equiv \begin{pmatrix} e^{\langle \ln \rho_{11}(\omega) \rangle} & \cdots & 0 \\ \cdot & \cdot & \cdot \\ \cdot & \cdot & \cdot \\ \cdot & \cdot & \cdot \\ 0 & \cdots & e^{\langle \ln \rho_{N_c N_c}(\omega) \rangle} \end{pmatrix}. \tag{A1}$$

In Figure A1, we then compare the $N_c = 8$ results for the TDOS(ω) obtained with the "full" ansatz (Equation (2)) and the "local" ansatz (Equation (A1)) calculated at several values of the disorder strength: $W = 8.0, 10, 12, 14$. Our data indicate that the majority of the contribution to the TDOS(ω) is actually coming from the local terms in Equation (2). The critical behavior at the Fermi level ($\omega = 0$) is the same for both the "local" and the "full" ansatz. However, the non-local contribution seems to be important for properly capturing the mobility edge behavior (marked by vertical arrows in Figure A1). Here, at the mobility edges, we observe the most pronounced difference between the TDOS(ω) obtained using the "local" and the "full" ansatz. These results indicate that, while the critical behavior at the band center is captured properly by the "local" ansatz, the mobility edge trajectories of the "local" ansatz, however, will converge slower with the cluster size N_c. To demonstrate this explicitly, in Figure A2 (left panel), we plot the typical density of states as a function of disorder strength W at the band center (TDOS($\omega = 0$)). The critical value of disorder strength (W_c) at which the TDOS($\omega = 0$) $= 0$ vanishes at the band center is the same for

both local and non-local ansatzes. However, as shown in the right panel of Figure A2, there is a substantial difference in the phase boundary near the band edges. Specifically, with the off-diagonal components, the re-entrance effect is much more pronounced even if the cluster size is relatively small. The off-diagonal components provide the contribution from the scattering among multiple sites, and hence generate more accurate results which are much closer to the results from the highly accurate transfer matrix method.

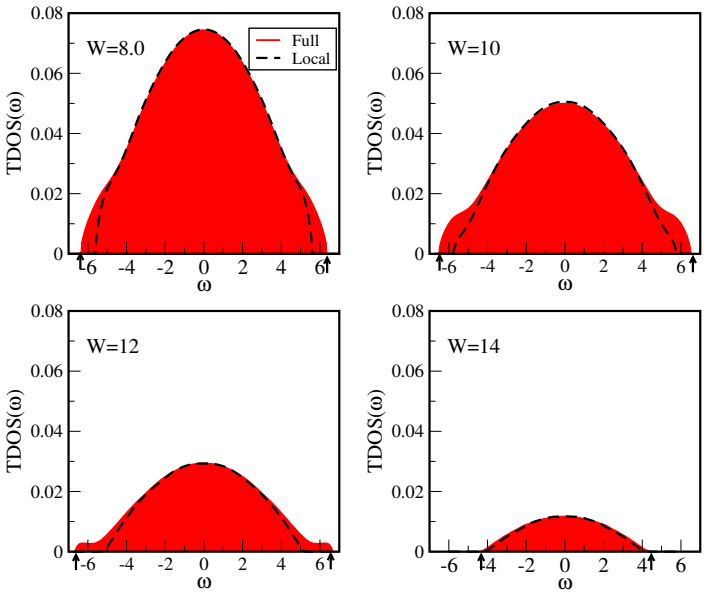

Figure A1. $N_c = 8$ results for the TDOS(ω) at increasing disorder strengths $W = 8, 10, 12, 14$. The data for the TDOS obtained using the "full" ansatz of Equation (2) (red shaded region), and the TDOS curves obtained using the simplified "local" ansatz of Equation (A1) (dashed lines), where the off-diagonal non-local contributions are set to zero. Vertical arrows mark the mobility edge boundaries.

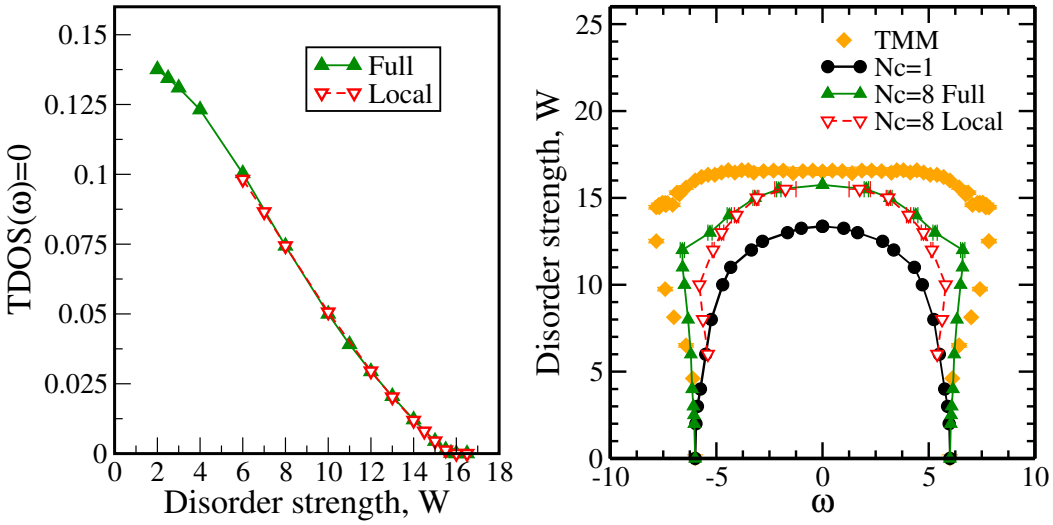

Figure A2. (**Left**): $N_c = 8$ cluster $TDOS(w = 0)$ vs disorder strength W calculated using the "full" (Equation (2)) and "local" (Equation (A1)) ansatzes. (**Right**): Disorder strength W vs. frequency ω phase diagram for the 3D Anderson model for $N_c = 1$ and $N_c = 8$ clusters. The mobility edge boundaries for $N_c = 8$ clusters are obtained using the "full" and "local" ansatzes. The transfer matrix method (TMM) mobility edge boundaries are taken from Ref. [52].

References

1. Anderson, P.W. Absence of Diffusion in Certain Random Lattices. *Phys. Rev.* **1958**, *109*, 1492–1505. [CrossRef]
2. Abrahams, E. (Ed.) *50 Years of Anderson Localization*; World Scientific: Singapore, 2010.
3. Vollhardt, D.; Wölfle, P. Anderson Localization in $d <\sim 2$ Dimensions: A Self-Consistent Diagrammatic Theory. *Phys. Rev. Lett.* **1980**, *45*, 842–846. [CrossRef]
4. Vollhardt, D.; Wölfle, P. Diagrammatic, self-consistent treatment of the Anderson localization problem in $d \leq 2$ dimensions. *Phys. Rev. B* **1980**, *22*, 4666–4679. [CrossRef]
5. Kramer, B.; MacKinnon, A. Localization: Theory and experiment. *Rep. Prog. Phys.* **1993**, *56*, 1469. [CrossRef]
6. John, S. Electromagnetic Absorption in a Disordered Medium near a Photon Mobility Edge. *Phys. Rev. Lett.* **1984**, *53*, 2169–2172. [CrossRef]
7. John, S. Strong localization of photons in certain disordered dielectric superlattices. *Phys. Rev. Lett.* **1987**, *58*, 2486–2489. [CrossRef]
8. Wolf, P.E.; Maret, G. Weak Localization and Coherent Backscattering of Photons in Disordered Media. *Phys. Rev. Lett.* **1985**, *55*, 2696–2699. [CrossRef] [PubMed]
9. Albada, M.P.V.; Lagendijk, A. Observation of Weak Localization of Light in a Random Medium. *Phys. Rev. Lett.* **1985**, *55*, 2692–2695. [CrossRef] [PubMed]
10. Tsang, L.; Ishimaru, A. Backscattering enhancement of random discrete scatterers. *J. Opt. Soc. Am. A* **1984**, *1*, 836–839. [CrossRef]
11. Wiersma, D.S.; Bartolini, P.; Lagendijk, A.; Righini, R. Localization of light in a disordered medium. *Nature* **1997**, *390*, 671–673. [CrossRef]
12. Störzer, M.; Gross, P.; Aegerter, C.M.; Maret, G. Observation of the critical regime near Anderson localization of light. *Phys. Rev. Lett.* **2006**, *96*, 063904. [CrossRef] [PubMed]
13. Sperling, T.; Buehrer, W.; Aegerter, C.M.; Maret, G. Direct determination of the transition to localization of light in three dimensions. *Nat. Photonics* **2013**, *7*, 48–52. [CrossRef]
14. Skipetrov, S.; Page, J.H. Red light for Anderson localization. *New J. Phys.* **2016**, *18*, 021001. [CrossRef]
15. Skipetrov, S.E.; Sokolov, I.M. Absence of Anderson Localization of Light in a Random Ensemble of Point Scatterers. *Phys. Rev. Lett.* **2014**, *112*, 023905. [CrossRef]
16. Sperling, T.; Schertel, L.; Ackermann, M.; Aubry, G.J.; Aegerter, C.M.; Maret, G. Can 3D light localization be reached in 'white paint'? *New J. Phys.* **2016**, *18*, 013039. [CrossRef]
17. Ángel, J.C.; Guzmán, J.T.; de Anda, A.D. Anderson localization of flexural waves in disordered elastic beams. *Sci. Rep.* **2019**, *9*, 3572. [CrossRef] [PubMed]
18. Frank, R.; Lubatsch, A.; Kroha, J. Theory of strong localization effects of light in disordered loss or gain media. *Phys. Rev. B* **2006**, *73*, 245107. [CrossRef]
19. Lubatsch, A.; Frank, R. Self-consistent quantum field theory for the characterization of complex random media by short laser pulses. *Phys. Rev. Res.* **2020**, *2*, 013324. [CrossRef]
20. Razo-López, L.; Fernández-Marín, A.; Méndez-Bermúdez, J.; Sánchez-Dehesa, J.; Gopar, V. Delay time of waves performing Lévy walks in 1D random media. *Sci. Rep.* **2020**, *10*, 20816. [CrossRef]
21. Kostadinova, E.G.; Padgett, J.L.; Liaw, C.D.; Matthews, L.S.; Hyde, T.W. Numerical study of anomalous diffusion of light in semicrystalline polymer structures. *Phys. Rev. Res.* **2020**, *2*, 043375. [CrossRef]
22. Ziegler, K. Ray Modes in Random Gap Systems. *Ann. Phys.* **2017**, *529*, 1600345. [CrossRef]
23. Leseur, O.; Pierrat, R.; Sáenz, J.J.; Carminati, R. Probing two-dimensional Anderson localization without statistics. *Phys. Rev. A* **2014**, *90*, 053827. [CrossRef]
24. Chabé, J.; Rouabah, M.T.; Bellando, L.; Bienaimé, T.; Piovella, N.; Bachelard, R.; Kaiser, R. Coherent and incoherent multiple scattering. *Phys. Rev. A* **2014**, *89*, 043833. [CrossRef]
25. Mafi, A.; Karbasi, S.; Koch, K.W.; Hawkins, T.; Ballato, J. Transverse Anderson Localization in Disordered Glass Optical Fibers: A Review. *Materials* **2014**, *7*, 5520–5527. [CrossRef] [PubMed]
26. White, D.H.; Haase, T.A.; Brown, D.J.; Hoogerland, M.D.; Najafabadi, M.S.; Helm, J.L.; Gies, C.; Schumayer, D.; Hutchinson, D.A.W. Observation of two-dimensional Anderson localisation of ultracold atoms. *Nat. Commun.* **2020**, *11*, 4942. [CrossRef] [PubMed]
27. Abou-Chacra, R.; Thouless, D.J.; Anderson, P.W. A Selfconsistent Theory of Localization. *J. Phys. C Solid State Phys.* **1973**, *6*, 1734–1752. [CrossRef]
28. Soven, P. Coherent-Potential Model of Substitutional Disordered Alloys. *Phys. Rev.* **1967**, *156*, 809–813. [CrossRef]
29. Shiba, H. A Reformulation of the Coherent Potential Approximation and Its Applications. *Prog. Theor. Phys.* **1971**, *46*, 77. [CrossRef]
30. Velický, B.; Kirkpatrick, S.; Ehrenreich, H. Single-Site Approximations in the Electronic Theory of Simple Binary Alloys. *Phys. Rev.* **1968**, *175*, 747–766. [CrossRef]
31. Kirkpatrick, S.; Velický, B.; Ehrenreich, H. Paramagnetic NiCu Alloys: Electronic Density of States in the Coherent-Potential Approximation. *Phys. Rev. B* **1970**, *1*, 3250–3263. [CrossRef]
32. Onodera, Y.; Toyozawa, Y. Persistence and Amalgamation Types in the Electronic Structure of Mixed Crystals. *J. Phys. Soc. Jpn.* **1968**, *24*, 341–355. [CrossRef]

33. Taylor, D. Vibrational Properties of Imperfect Crystals with Large Defect Concentrations. *Phys. Rev.* **1967**, *156*, 1017–1029. [CrossRef]
34. Yonezawa, F. A Systematic Approach to the Problems of Random Lattices. I: A Self-Contained First-Order Approximation Taking into Account the Exclusion Effect. *Prog. Theor. Phys.* **1968**, *40*, 734–757. [CrossRef]
35. Weh, A.; Zhang, Y.; Östlin, A.; Terletska, H.; Bauernfeind, D.; Tam, K.M.; Evertz, H.G.; Byczuk, K.; Vollhardt, D.; Chioncel, L. Dynamical mean-field theory of the Anderson-Hubbard model with local and nonlocal disorder in tensor formulation. *Phys. Rev. B* **2021**, *104*, 045127. [CrossRef]
36. Dobrosavljević, V.; Pastor, A.A.; Nikolić, B.K. Typical medium theory of Anderson localization: A local order parameter approach to strong-disorder effects. *EPL Europhys. Lett.* **2003**, *62*, 76. [CrossRef]
37. Schubert, G.; Schleede, J.; Byczuk, K.; Fehske, H.; Vollhardt, D. Distribution of the local density of states as a criterion for Anderson localization: Numerically exact results for various lattices in two and three dimensions. *Phys. Rev. B* **2010**, *81*, 155106. [CrossRef]
38. Byczuk, K.; Hofstetter, W.; Vollhardt, D. Mott-Hubbard Transition versus Anderson Localization in Correlated Electron Systems with Disorder. *Phys. Rev. Lett.* **2005**, *94*, 056404. [CrossRef] [PubMed]
39. Semmler, D.; Byczuk, K.; Hofstetter, W. Mott-Hubbard and Anderson metal-insulator transitions in correlated lattice fermions with binary disorder. *Phys. Rev. B* **2010**, *81*, 115111. [CrossRef]
40. Murphy, N.C.; Wortis, R.; Atkinson, W.A. Generalized inverse participation ratio as a possible measure of localization for interacting systems. *Phys. Rev. B* **2011**, *83*, 184206. [CrossRef]
41. Aguiar, M.C.O.; Dobrosavljević, V.; Abrahams, E.; Kotliar, G. Critical Behavior at the Mott-Anderson Transition: A Typical-Medium Theory Perspective. *Phys. Rev. Lett.* **2009**, *102*, 156402. [CrossRef]
42. Aguiar, M.C.O.; Dobrosavljević, V. Universal Quantum Criticality at the Mott-Anderson Transition. *Phys. Rev. Lett.* **2013**, *110*, 066401. [CrossRef]
43. Oliveira, W.S.; Aguiar, M.C.O.; Dobrosavljević, V. Mott-Anderson transition in disordered charge-transfer model: Insights from typical medium theory. *Phys. Rev. B* **2014**, *89*, 165138. [CrossRef]
44. Bragança, H.; Aguiar, M.C.O.; Vučičević, J.; Tanasković, D.; Dobrosavljević, V. Anderson localization effects near the Mott metal-insulator transition. *Phys. Rev. B* **2015**, *92*, 125143. [CrossRef]
45. Dobrosavljević, V. Typical-Medium Theory of Mott–Anderson Localization. *Int. J. Mod. Phys. B* **2010**, *24*, 1680–1726. [CrossRef]
46. Byczuk, K.; Hofsletter, W.; Yu, U.; Vollhardt, D. Correlated electrons in the presence of disoder. *Eur. Phys. J. Spec. Top.* **2009**, *180*, 135–151. [CrossRef]
47. Byczuk, K.; Hofstetter, W.; Vollhardt, D. Anderson Localization VS. Mott-Hubbard Metal-Insulator Transition in Disordered, Interacting Lattice Fermion Systems. *Int. J. Mod. Phys. B* **2010**, *24*, 1727–1755. [CrossRef]
48. Alvermann, A.; Schubert, G.; Weiße, A.; Bronold, F.; Fehske, H. Characterisation of Anderson localisation using distribution. *Phys. B Condens. Matter* **2005**, *359–361*, 789–791. [CrossRef]
49. Janssen, M. Mutifractal Analysis of Broadly Distributed Observables at Criticality. *Int. J. Mod. Phys. B* **1994**, *8*, 943. [CrossRef]
50. Janssen, M. Statistics and scaling in disordered mesoscopic electronic systems. *Phys. Rep.* **1998**, *295*, 1–91. [CrossRef]
51. Logan, D.E.; Wolynes, P.G. Dephasing and Anderson localization in topologically disordered systems. *Phys. Rev. B* **1987**, *36*, 4135–4147. [CrossRef]
52. Ekuma, C.E.; Terletska, H.; Tam, K.M.; Meng, Z.Y.; Moreno, J.; Jarrell, M. Typical medium dynamical cluster approximation for the study of Anderson localization in three dimensions. *Phys. Rev. B* **2014**, *89*, 081107. [CrossRef]
53. Ekuma, C.E.; Moore, C.; Terletska, H.; Tam, K.M.; Moreno, J.; Jarrell, M.; Vidhyadhiraja, N.S. Finite-cluster typical medium theory for disordered electronic systems. *Phys. Rev. B* **2015**, *92*, 014209. [CrossRef]
54. Terletska, H.; Zhang, Y.; Tam, K.M.; Berlijn, T.; Chioncel, L.; Vidhyadhiraja, N.; Jarrell, M. Systematic quantum cluster typical medium method for the study of localization in strongly disordered electronic systems. *Appl. Sci.* **2018**, *8*, 2401. [CrossRef]
55. Jarrell, M.; Krishnamurthy, H.R. Systematic and causal corrections to the coherent potential approximation. *Phys. Rev. B* **2001**, *63*, 125102. [CrossRef]
56. Jarrell, M.; Maier, T.; Huscroft, C.; Moukouri, S. Quantum Monte Carlo algorithm for nonlocal corrections to the dynamical mean-field approximation. *Phys. Rev. B* **2001**, *64*, 195130. [CrossRef]
57. Sen, S.; Terletska, H.; Moreno, J.; Vidhyadhiraja, N.S.; Jarrell, M. Local theory for Mott-Anderson localization. *Phys. Rev. B* **2016**, *94*, 235104. [CrossRef]
58. Terletska, H.; Zhang, Y.; Chioncel, L.; Vollhardt, D.; Jarrell, M. Typical-medium multiple-scattering theory for disordered systems with Anderson localization. *Phys. Rev. B* **2017**, *95*, 134204. [CrossRef]
59. Terletska, H.; Ekuma, C.E.; Moore, C.; Tam, K.M.; Moreno, J.; Jarrell, M. Study of off-diagonal disorder using the typical medium dynamical cluster approximation. *Phys. Rev. B* **2014**, *90*, 094208. [CrossRef]
60. Mondal, W.R.; Berlijn, T.; Jarrell, M.; Vidhyadhiraja, N.S. Phonon localization in binary alloys with diagonal and off-diagonal disorder: A cluster Green's function approach. *Phys. Rev. B* **2019**, *99*, 134203. [CrossRef]
61. Mondal, W.R.; Vidhyadhiraja, N.S. Effect of short-ranged spatial correlations on the Anderson localization of phonons in mass-disordered systems. *Bull. Mater. Sci.* **2020**, *43*, 314. [CrossRef]
62. Zhang, Y.; Terletska, H.; Moore, C.; Ekuma, C.; Tam, K.M.; Berlijn, T.; Ku, W.; Moreno, J.; Jarrell, M. Study of multiband disordered systems using the typical medium dynamical cluster approximation. *Phys. Rev. B* **2015**, *92*, 205111. [CrossRef]

63. Zhang, Y.; Nelson, R.; Siddiqui, E.; Tam, K.M.; Yu, U.; Berlijn, T.; Ku, W.; Vidhyadhiraja, N.S.; Moreno, J.; Jarrell, M. Generalized multiband typical medium dynamical cluster approximation: Application to (Ga,Mn)N. *Phys. Rev. B* **2016**, *94*, 224208. [CrossRef]
64. Zhang, Y.; Nelson, R.; Tam, K.M.; Ku, W.; Yu, U.; Vidhyadhiraja, N.S.; Terletska, H.; Moreno, J.; Jarrell, M.; Berlijn, T. Origin of localization in Ti-doped Si. *Phys. Rev. B* **2018**, *98*, 174204. [CrossRef]
65. Östlin, A.; Zhang, Y.; Terletska, H.; Beiuşeanu, F.; Popescu, V.; Byczuk, K.; Vitos, L.; Jarrell, M.; Vollhardt, D.; Chioncel, L. Ab initio typical medium theory of substitutional disorder. *Phys. Rev. B* **2020**, *101*, 014210. [CrossRef]
66. Zhang, Y.; Terletska, H.; Tam, K.M.; Wang, Y.; Eisenbach, M.; Chioncel, L.; Jarrell, M. Locally self-consistent embedding approach for disordered electronic systems. *Phys. Rev. B* **2019**, *100*, 054205. [CrossRef]
67. Terletska, H.; Moilanen, A.; Tam, K.M.; Zhang, Y.; Wang, Y.; Eisenbach, M.; Vidhyadhiraja, N.; Chioncel, L.; Moreno, J. Non-local corrections to the typical medium theory of Anderson localization. *Ann. Phys.* **2021**, 168454. [CrossRef]
68. Tam, K.M.; Zhang, Y.; Terletska, H.; Wang, Y.; Eisenbach, M.; Chioncel, L.; Moreno, J. Application of the locally self-consistent embedding approach to the Anderson model with non-uniform random distributions. *Ann. Phys.* **2021**, 168480. [CrossRef]
69. Georges, A.; Kotliar, G.; Krauth, W. Superconductivity in the Two-Band Hubbard Model in Infinite Dimensions. *Z. Phys. B Condens. Matter* **1993**, *92*, 313–321. [CrossRef]
70. Biroli, G.; Kotliar, G. Cluster methods for strongly correlated electron systems. *Phys. Rev. B* **2002**, *65*, 155112. [CrossRef]
71. Biroli, G.; Parcollet, O.; Kotliar, G. Cluster dynamical mean-field theories: Causality and classical limit. *Phys. Rev. B* **2004**, *69*, 205108. [CrossRef]
72. Kotliar, G.; Savrasov, S.; Palsson, G.; Biroli, G. Cellular Dynamical Mean Field Approach to Strongly Correlated Systems. *Phys. Rev. Lett.* **2001**, *87*, 186401. [CrossRef]
73. Lichtenstein, A.I.; Katsnelson, M.I. Antiferromagnetism and d-wave superconductivity in cuprates: A cluster dynamical mean-field theory. *Phys. Rev. B* **2000**, *62*, R9283–R9286. [CrossRef]
74. Bulka, B.; Kramer, B.; MacKinnon, A. Mobility edge in the three-dimensional Anderson model. *Z. Phys. B Condens. Matter* **1985**, *60*, 13–17. [CrossRef]
75. Li, J.; Chu, R.L.; Jain, J.K.; Shen, S.Q. Topological Anderson Insulator. *Phys. Rev. Lett.* **2009**, *102*, 136806. [CrossRef]
76. Yonezawa, F.; Morigaki, K. Coherent Potential Approximation. Basic concepts and applications. *Prog. Theor. Phys. Supp.* **1973**, *53*, 1–76. [CrossRef]
77. Georges, A.; Kotliar, G.; Krauth, W.; Rozenberg, M. Dynamical mean-field theory of strongly correlated fermion systems and the limit of infinite dimensions. *Rev. Mod. Phys.* **1996**, *68*, 13–125. [CrossRef]
78. Maier, T.; Jarrell, M.; Pruschke, T.; Hettler, M.H. Quantum cluster theories. *Rev. Mod. Phys.* **2005**, *77*, 1027–1080. [CrossRef]
79. Lee, P.A.; Ramakrishnan, T.V. Disordered electronic systems. *Rev. Mod. Phys.* **1985**, *57*, 287–337. [CrossRef]
80. Selvan, R.; Genish, I.; Perelshtein, I.; Moreno, J.; Gedanken, A. Single step, low temperature synthesis of submicron-sized rare earth hexaborides. *J. Phys. Chem. C* **2008**, *112*, 1795. [CrossRef]
81. Bulka, B.; Schreibe, M.; Kramer, B. Localization, Quantum Interference, and the Metal-Insulator Transition. *Z. Phys. B* **1987**, *66*, 21–30. [CrossRef]
82. Kramer, B.; Schreiber, M. Localization, quantum interference and transport in disordered solids. In *Fluctuations and Stochastic Phenomena in Condensed Matter*; Lecture Notes in Physics; Garrido, L., Ed.; Springer: Berlin/Heidelberg, Germany, 1987; Volume 268, pp. 351–375. [CrossRef]
83. Kramer, B.; MacKinnon, A.; Ohtsuki, T.; Slevin, K. Finite Size Scaling Analysis of the Anderson Transition. *Int. J. Mod. Phys. B* **2010**, *24*, 1841–1854. [CrossRef]
84. Rodriguez, A.; Vasquez, L.J.; Slevin, K.; Römer, R.A. Critical Parameters from a Generalized Multifractal Analysis at the Anderson Transition. *Phys. Rev. Lett.* **2010**, *105*, 046403. [CrossRef]
85. Rodriguez, A.; Vasquez, L.J.; Slevin, K.; Römer, R.A. Multifractal finite-size scaling and universality at the Anderson transition. *Phys. Rev. B* **2011**, *84*, 134209. [CrossRef]
86. Slevin, K.; Ohtsuki, T. Numerical verification of universality for the Anderson transition. *Phys. Rev. B* **2001**, *63*, 045108. [CrossRef]
87. Slevin, K.; Ohtsuki, T. Critical exponent for the Anderson transition in the three-dimensional orthogonal universality class. *New J. Phys.* **2014**, *16*, 015012. [CrossRef]
88. Slevin, K.; Ohtsuki, T. Corrections to Scaling at the Anderson Transition. *Phys. Rev. Lett.* **1999**, *82*, 382–385. [CrossRef]
89. Chang, T.; Bauer, J.D.; Skinner, J.L. Critical exponents for Anderson localization. *J. Chem. Phys.* **1990**, *93*, 8973–8982. [CrossRef]
90. MacKinnon, A.; Kramer, B. The scaling theory of electrons in disordered solids: Additional numerical results. *Z. Phys. B Condens. Matter* **1983**, *53*, 1–13. [CrossRef]
91. de Queiroz, S.L.A. Reentrant behavior and universality in the Anderson transition. *Phys. Rev. B* **2001**, *63*, 214202. [CrossRef]
92. Grussbach, H.; Schreiber, M. Determination of the mobility edge in the Anderson model of localization in three dimensions by multifractal analysis. *Phys. Rev. B* **1995**, *51*, 663–666. [CrossRef]
93. Sénéchal, D. An introduction to quantum cluster methods. *arXiv* **2010**, arXiv:0806.2690.
94. Kraberger, G.J.; Triebl, R.; Zingl, M.; Aichhorn, M. Maximum entropy formalism for the analytic continuation of matrix-valued Green's functions. *Phys. Rev. B* **2017**, *96*, 155128. [CrossRef]
95. Rowlands, D.A. Investigation of the nonlocal coherent-potential approximation. *J. Phys. Condens. Matter* **2006**, *18*, 3179–3195. [CrossRef]

96. Zhang, Y.; Zhang, Y.F.; Yang, S.X.; Tam, K.M.; Vidhyadhiraja, N.S.; Jarrell, M. Calculation of two-particle quantities in the typical medium dynamical cluster approximation. *Phys. Rev. B* **2017**, *95*, 144208. [CrossRef]
97. Roy, B.; Slager, R.J.; Juričić, V. Global Phase Diagram of a Dirty Weyl Liquid and Emergent Superuniversality. *Phys. Rev. X* **2018**, *8*, 031076. [CrossRef]